ACS OMEGA

Article

http://pubs.acs.org/journal/acsodf

Water Adsorption Properties of NOTT-401 and CO_2 Capture under Humid Conditions

Elí Sánchez-González,[†] J. Raziel Álvarez,[†] Ricardo A. Peralta,[†] Alberto Campos-Reales-Pineda,[†] Adriana Tejeda-Cruz,[†] Enrique Lima,[†] Jorge Balmaseda,[†] Eduardo González-Zamora,*[,‡] and Ilich A. Ibarra*[,†]

[†]Instituto de Investigaciones en Materiales, Universidad Nacional Autónoma de México, Circuito Exterior s/n, CU, Del. Coyoacán, 04510 Ciudad de México, Mexico

[‡]Departamento de Química, Universidad Autónoma Metropolitana-Iztapalapa, San Rafael Atlixco 186, Col. Vicentina, Iztapalapa, C. P. 09340 Ciudad de México, Mexico

Supporting Information

ABSTRACT: The water-stable material NOTT-401 was investigated for CO_2 capture under humid conditions. Water adsorption properties of NOTT-401 were studied, and their correlation with CO_2 sequestration at different relative humidities (RHs) showed that the CO_2 capture increased from 1.2 wt % (anhydrous conditions) to 3.9 wt % under 5% RH at 30 °C, representing a 3.2-fold improvement.

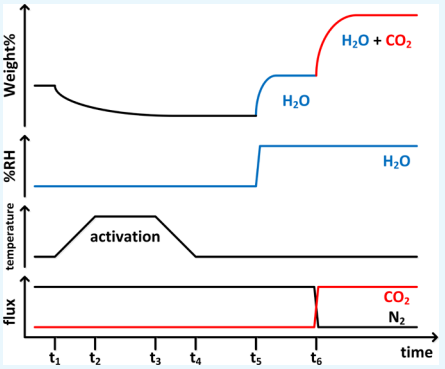

INTRODUCTION

Last year, global CO_2 emissions have increased up to 35.7 billion tons, of which 90% are fuel-combustion-related emissions.[1] As other porous materials, porous coordination polymers (PCPs) have stepped up to the challenge of CO_2 sequestration; they are known for their adsorption properties and in particular for the feasibility of tuning their pore shape, size, and adsorption enthalpies. Potential industrial applications for PCP materials (such as the treatment of postcombustion flue gas where 5−7% of its composition is water) need to show high adsorption CO_2 capacity and water stability.[2]

Some representative examples of PCPs that showed water stability are MIL-53, MIL-100, MIL-101, MIL-110, and ZIF-8.[3] Water stability in PCPs relies on the metal−ligand bond strength and steric effects around the ligand.[4] Lillerud et al.[5] introduced a water-stable material entitled UiO-66, whereas Yaghi and co-workers showed a Zr-based water-stable family of PCPs.[6] Recently, Snurr, Hupp, and Farha have developed a water-stable series of Zr-based PCPs (NU-1101 to 1105) with ultrahigh surface areas.[7] One of the most common strategies to improve the water stability of PCPs is ligand functionalization. Walton et al.[8] modified a Zr-based PCP series by adding nonpolar groups to the ligand. Another synthetic approach to functionalization is to decorate the PCPs with amines such as HNUST-4,[9] MIL-101,[10] and MOF-74/CPO-27.[11]

Studies on CO_2 adsorption in the presence of water molecules were first presented by Férey et al.[12,12a] and later by Snurr and co-workers.[12b] Because H_2O molecules strongly compete with CO_2 for adsorption sites, the overall CO_2 capture is often decreased. However, Llewellyn and co-workers reported an exceptional increase (5-fold) in the CO_2 adsorption in MIL-100(Fe) at 40% relative humidity (RH).[13] Additionally, Yaghi et al.[6] demonstrated that the incorporation of bridged μ_3-OH groups within the pores of PCPs increases water affinity. Hence, we hypothesized that the incorporation of functional groups within the PCP pores (such as −OH) can be an effective strategy to enhance the water stability of PCPs.

Thus, herein we have chosen a material entitled NOTT-401[14] that shows μ_2-OH functional groups inside of the channels (see Figure 1). NOTT-401 crystallizes in the tetragonal space group $I4_1/amd$, and it is based on a binuclear [$Sc_2(\mu_2$-OH)] building block and 2,5-thiophenedicarboxylate (Figure S1). The Sc(III) center adopts an octahedral coordination environment, constructed by two adjacent μ_2-OH groups and four different 2,5-thiophenecarboxylate O-donors. The three-dimensional NOTT-401 framework (see Figure 1) comprises channel openings of approximately 6.3 Å (van der Waals radii).[14]

Received: June 29, 2016
Accepted: August 16, 2016
Published: August 30, 2016

DOI: 10.1021/acsomega.6b00102
ACS Omega 2016, 1, 305−310

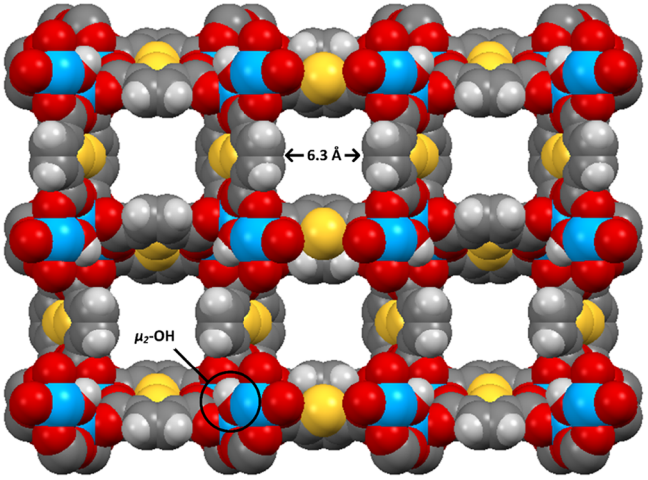

Figure 1. View of the crystalline structure of NOTT-401 along the *c*-axis, showing 6.3 Å channels (Sc: blue; S: yellow; O: red; C: grey; H: white).

EXPERIMENTAL SECTION

Synthesis of NOTT-401 was carried out as previously reported elsewhere.[14] The synthesized product was first analyzed using powder X-ray diffraction (PXRD). PXRD patterns were collected using a Bruker AXD D8 Advance diffractometer under ambient conditions, operated at 160 W (40 kV and 40 mA) for Cu Kα_1 (λ = 1.5406 Å). Thermal gravimetric analyses were carried out on a Q500HR analyzer (TA Instruments) under an N_2 atmosphere at a scan rate of 2 °C min^{-1}. Nitrogen (N_2) adsorption isotherms were performed using a Micromeritics ASAP 2020 sorptometer (volumetric technique). On the basis of the N_2 adsorption data, it was possible to estimate the Brunauer–Emmett–Teller (BET) surface area (0.01 < P/P_0 < 0.04). Static CO_2 adsorption isotherms, from 0 to 15 bar at 30 °C, were obtained on a BELSORP-HP analyzer. CO_2 experiments under dynamic and isothermal (30 °C) conditions were carried out using a humidity-controlled thermobalance (TA Instruments, model Q5000SA) by varying the RH.

Kinetic CO_2 Capture Experiments. Kinetic CO_2 uptake experiments were carried out using a thermobalance (Q500 HR, TA Instruments). Before measurements, NOTT-401 samples were activated at 180 °C for 1 h inside of the thermobalance under a constant N_2 flow. After the activation, the samples were cooled down to 30 °C, and then CO_2 uptake experiments were performed under a constant CO_2 flow of 60 mL min^{-1}. Then, a series of fixed humidity-controlled experiments were carried out using the thermobalance (Q5000SA, TA Instruments). As mentioned earlier, the samples were activated before each experiment (180 °C for 1 h under a N_2 flow). Then, the kinetic uptake experiments were carried out at 30 °C, under a CO_2 flow of 60 mL min^{-1} and a fixed RH (see Scheme S1).

Water Adsorption Experiments. Isotherms were recorded using a DVS Advantage 1 instrument (Surface Measurement Systems) by a dynamic method, with air as the carrier gas (mass sensitivity: 0.1 μg, RH accuracy: 0.5% RH, and vapor pressure accuracy: 0.7% P/P_0). Before measurements, samples were activated at 180 °C for 2 h under an N_2 flow. The water uptake in weight percentage (wt %) units was calculated as [(adsorbed amount of water)/(amount of adsorbent) × 100], consistent with established procedures.

RESULTS AND DISCUSSION

After the synthesis of NOTT-401, free-solvent molecules remain in the pores. Thus, to gain accessibility to the pores upon activation (heating under vacuum), these molecules were exchanged for acetone. The NOTT-401 stability was assessed using thermogravimetric analysis (TGA) (see Figure S2) and bulk PXRD experiments (see Figure S3) before and after the activation process. Both PXRD experiments showed retention of the structural integrity of NOTT-401. Nitrogen (N_2) adsorption isotherms were performed for the activated NOTT-401 samples (180 °C and 10^{-5} bar for 2 h), and with this information, a BET surface area of 1504 m^2 g^{-1} and a pore volume of 0.66 cm^3 g^{-1} were calculated in the range of 0.01 < P/P_0 < 0.04. Water adsorption isotherms were carried out on the activated NOTT-401 samples (180 °C for 2 h under an N_2 flow) at 20 and 30 °C (see Experimental Section). Figure 2

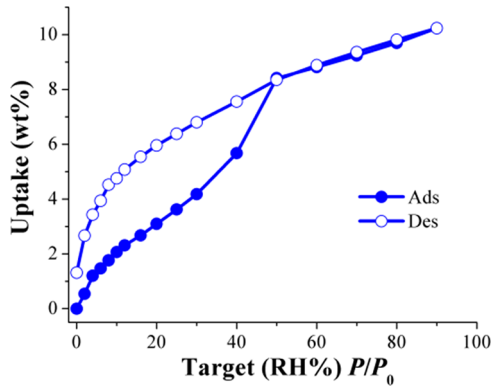

Figure 2. Water adsorption isotherm of NOTT-401 at 30 °C. Solid circles correspond to adsorption, and open circles correspond to desorption.

shows the water (H_2O) adsorption isotherm of NOTT-401 at 30 °C. This adsorption isotherm exhibits an uptake of H_2O that gradually increases as the pressure increases up to approximately $\%P/P_0$ = 30. Then, a relatively fast increase in the adsorbed amount of H_2O was observed from $\%P/P_0$ = 30 to 50. At the end of the experiment, from $\%P/P_0$ = 50 to 90, a constant lineal H_2O uptake was observed, with a maximum water uptake of approximately 10.2 wt %. The overall H_2O isotherm shape for NOTT-401 is characteristic of a functionalized PCP material with hydroxyl groups,[6] and from $\%P/P_0$ = 0 to 50, a marked hysteresis loop was observed with a sheer drop in the desorption phase (Figure 2, open circles). The diameter of the pores in NOTT-401 is approximately 6.3 Å,[14] which is considerably larger than the kinetic diameter of H_2O (~2.7 Å). Hence, the characteristic "kinetic trap" description cannot be used for the hysteresis loop.[15] In this case, this hysteresis can be attributed to the relatively strong host–guest interactions that provide an enhanced water affinity to NOTT-401. We then propose that these interactions are the result of H_2O molecules forming hydrogen bonds with the μ_2-OH functional groups in the inner surface of the NOTT-401 pores, as previously reported.[16]

We previously reported on the water adsorption properties of NOTT-400,[19d] which is not isostructural to NOTT-401 but is constructed with the same binuclear [$Sc_2(\mu_2$-OH)] building block. Interestingly, the water adsorption isotherm of NOTT-400 is very different than that exhibited by NOTT-401. Although these two materials share the same hydrophilic μ_2-

DOI: 10.1021/acsomega.6b00102
ACS Omega 2016, 1, 305–310

OH functional group, NOTT-400 is considerably more hydrophobic than NOTT-401. Because NOTT-400 is constructed with a more hydrophobic ligand (H_4BPTC = biphenyl-3,3′,5,5′-tetracarboxylic acid) than 2,5-thiophenedicarboxylic acid (NOTT-401), at low $\%P/P_0$, the water uptake for NOTT-400 is considerably lower than that for NOTT-401.[19d] Thus, we may conclude that the nature of the ligand that conforms a PCP controls the overall water adsorption process even though the same hydrophilic functional group (μ_2-OH) is present.

A second H_2O adsorption isotherm (at 20 °C) was performed to calculate the isosteric heat of adsorption (enthalpy) for water (see Figure S4). This was calculated by fitting the two adsorption isotherms (20 and 30 °C) to the Clausius−Clapeyron equation (see Supporting Information). The enthalpy value was estimated to be 60.7 kJ mol^{-1}, which is a characteristic value for PCPs,[4a] and the magnitude represents a very strong hydrogen bond between water and the μ_2-OH functional groups inside of the NOTT-401 channels.

Later, dynamic and isothermal NOTT-401 CO_2 capture experiments were carried out. The kinetic CO_2 uptake experiment at 30 °C is presented in Figure 3. Under anhydrous

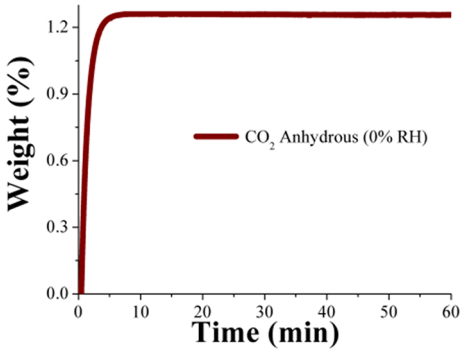

Figure 3. Kinetic CO_2 uptake experiment performed under anhydrous conditions of 30 °C with a 60 mL min^{-1} CO_2 flow.

conditions and at 30 °C, the CO_2 uptake promptly reached its maximum just after 7 min; it was estimated to be 1.2 wt % and remained stable through the rest of the experiment (60 min). Additionally, CO_2 sorption experiments were performed on NOTT-401 under static and isothermal conditions of 30 °C and 1 bar (see Figure S5). The total CO_2 uptake was 11.3 wt %, which is one order of magnitude higher than that obtained under dynamic conditions (1.2 wt %). This result is reasonable because under static conditions, the stabilization time for each measurement (the gradual increase in the CO_2 pressure) is much longer than that under dynamic conditions where there is a rapid flow of CO_2 gas (60 mL min^{-1}), and therefore the CO_2 uptake is also higher. In addition, the pretreatment of the samples is completely different in each experiment. Under dynamic conditions, the activation is generated by heating at 180 °C for 1 h under a nitrogen flow. When this activation is finished, the temperature is cooled down to 30 °C (under N_2) and then the samples were subjected to a flow of CO_2. This means that the sample is filled with N_2 molecules, which are eventually displaced by CO_2 molecules. On the other hand, in a static CO_2 adsorption experiment, the sample is activated under vacuum (10^{-3} bar) at 180 °C for 1 h, providing a completely empty material. Thus, when "small" amounts of CO_2 enter into the pores of NOTT-401, there is nothing to displace (N_2 molecules), and therefore the total uptake is expected to be much higher than under dynamic conditions, as previously reported.[19,19e] Nevertheless, the central target of this study is to come closer to a more lifelike CO_2 capture state (constant CO_2 flow) and analyze the effect of small amounts of water on the overall CO_2 capture.

Henry's law applies in adsorbate−adsorbent systems where the adsorbate is too dilute that there is neither competition for adsorption sites nor interaction between adsorbate molecules.[17,17a] The experimental CO_2 adsorption isotherm of NOTT-401 (at 30 °C) obeys this law, suggesting the ideal gas behavior of CO_2 within the pores (see Figure S6). This is possible when the thermal energy of the CO_2 molecules exceeds the potential energies of the dispersive and the quadrupole interactions with the pore surface. The absence of load centers with intensive electric fields in the framework as well as the proximity between the adsorption experiment (30 °C) and the adsorbate critical temperatures[17b] (31 °C) can explain such ideal behavior.

The behavior of the H_2O adsorption isotherm is much more complex. The large hysteresis loop at low pressure (Figure 2) suggests the existence of specific adsorption sites with strong interactions. NOTT-401 includes 16 μ_2-OH groups per unit cell.[14] These sites retain 65% of the limit capacity of the material. The strong dipolar interaction between them explains the hysteresis loop at low pressure. The behavior of NOTT-401 changes to being more hydrophobic after H_2O molecules entirely cover the μ_2-OH functional groups, generating the first adsorption domain (see Figure S7). Apparently, 2,5-thiophenedicarboxylate ligands are involved in the second adsorption domain. The hydrophobic nature of these building units and their high electron densities can open the possibility of retaining molecules with a high electron density which favor dispersive interactions.

Then, kinetic CO_2 isotherm experiments at 30 °C and under different RHs (5, 20, and 30% RH) were carried out. These RHs were selected according to the information obtained from the water adsorption isotherm (see Figure 2): these three RHs are in the low uptake region where the H_2O uptake slowly increases with increasing pressure.

First, for the fixed RH experiments, a NOTT-401 solvent-exchanged sample was activated at 180 °C for 1 h under a flow of N_2 gas (see Scheme S1). Then the sample was cooled down to 30 °C. When this temperature was stable, the RH was fixed at 5% RH, and after reaching equilibrium, the sample was exposed to a constant CO_2 flow of 60 mL min^{-1} (see Figure 4A). Figure 4A shows a constant uptake of water, which begins immediately at 0 min. Only after 20 min did the water uptake become steady. Interestingly, on the other hand, the stabilization time for the CO_2 uptake experiment under anhydrous conditions is reached in only one-third of this time, that is, 7 min (see Figure 3). This difference can be attributed to the diffusion coefficients; because the coefficient of the water molecule is smaller than that of CO_2, more time is required for water (vapor adsorption) to reach stability than for CO_2 (gas adsorption) in microporous materials.[18] After the H_2O uptake reached stability, the adsorption remained constant (plateau) from 20 to 53 min (1.0 wt %, in accordance with the H_2O adsorption isotherm; 1.1 wt %). Afterwards, the sample was exposed to a CO_2 flow (60 mL min^{-1}), and an abrupt weight increment was observed which stabilized at around 90 min (see Figure 4A). Our hypothesis is that the amount of adsorbed H_2O is unchanged after the dosing of H_2O/CO_2 mixed gas as we previously reported.[19] In the final part of the experiment, from 90 to 120 min , the maximum amount of CO_2

DOI: 10.1021/acsomega.6b00102
ACS Omega 2016, 1, 305−310

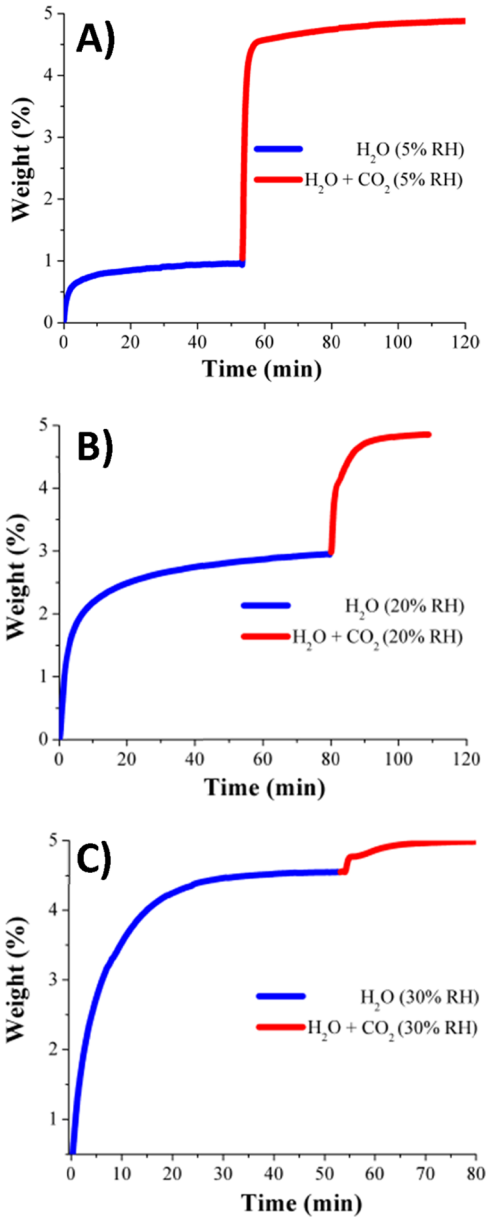

Figure 4. Kinetic CO_2 uptake experiments performed at 30 °C and a series of relative humidities: (A) 5, (B) 20, and (C) 30% RH; H_2O (blue line) and H_2O + CO_2 (red line).

captured was 3.9 wt % (contemplating the 1.0 wt % corresponding to the water uptake). Additionally, after this CO_2 capture experiment at 5% RH, a PXRD experiment was carried out to evaluate the retention of the crystallinity of NOTT-401, which can lead to the assessment of the sorbent regeneration. As expected (because NOTT-401 is a water-stable PCP), the material retained its crystallinity (Figure S8), suggesting that the regeneration of the material after it has been exposed to water (RH) is possible.

Hence, in the presence of 5% RH, the CO_2 capture was approximately 3.2-fold augmented (from 1.2 wt % to 3.9 wt %) when compared with anhydrous conditions. This improvement in the CO_2 uptake on account of H_2O can be rationalized by the CO_2 confinement effects produced by the water molecules.[20]

Nevertheless, it is important to consider the scenario (as a source of error) where CO_2 increases the H_2O uptake. For instance, in the bulk phase, it is very well known that CO_2 and H_2O participate in hydration reactions to form unstable carbonic acid and eventually dissociate into more stable ions ($CO_2 + H_2O \leftrightarrow H_2CO_3 \leftrightarrow HCO_3^- + H^+$).[21,21a,b] The formation of CO_2 hydrate involves a high critical pressure (from 20 to 200 bar) and subambient temperatures (273−285 K).[21c] Additionally, CO_2 solubility in H_2O is very low (0.0286 mol/kg of water) at 1 bar and 303.15 K.[21d] However, the adsorption of the binary mixture (CO_2 and H_2O) is known to be a very nonideal system where highly complex interactions between these two species and a pore surface take place.[21e−g] Thus, the pore-surface chemistry and the pore dimensions of the adsorbent (NOTT-401) play fundamental roles in modifying the loading of CO_2 on the adsorbed water layers at low CO_2 partial pressures (e.g., 1 bar), and a relatively small error could be associated that the CO_2 may also augment the water uptake. This negligible error can be attributed to a cooperative effect of the adsorption of CO_2 and the formation of its water complexes inside of the pores, augmenting the adsorbed water in a small portion.[21h]

On a more detailed inspection, CO_2 can be found to interact with field gradients generated by H_2O molecules. Certainly, the electron density from the oxygen atoms (H_2O molecules) favors their interaction with the dispersive 2,5-thiophenedicarboxylate building units in NOTT-401 (see Figure S9), and because H_2O has a smaller kinetic diameter (2.6 Å) than that of CO_2 (3.3 Å), this molecule diffuses easily through the narrow channels in NOTT-401 (6.3 Å). The Henry constants estimated from the CO_2 and H_2O adsorption isotherms are 0.003213 ± 0.000002 and 0.52 ± 0.03 mmol (g mmHg)$^{-1}$, respectively, at 30 °C (see Figures S6 and S11). Thus, NOTT-401 shows a selectivity for water in a $H_2O(v)-CO_2(v)$ mixture of 162 ± 9. This high selectivity to water prevents CO_2 from being absorbed preferentially in any adsorption domain. However, the high water selectivity allows the creation of stable domains in NOTT-401, which favor the CO_2 retention.

Later, kinetic CO_2 uptake experiments were carried out on an activated NOTT-401 sample at 30 °C, with a modified relative humidity of 20% RH (see Figure 4B). Figure 4B exhibits a regular H_2O weight increment that begins at the start of the experiment (0 min) and at around 50 min becomes steady. From 50 to 80 min, the H_2O adsorption remained constant, with an uptake of approximately 2.9 wt %, showing good agreement with the 3.0 wt % in the H_2O adsorption isotherm (see Figure 2). Then, a CO_2 flow was initiated, after which a sharp uptake was recorded (see Figure 4B). After achieving stability (at around 100 min), the final CO_2 uptake was 1.9 wt %. Therefore, the CO_2 capture was approximately 1.6-fold augmented (taking anhydrous conditions as reference). Finally, another set of kinetic CO_2 uptake experiments were performed on a NOTT-401 activated sample at 30 °C and 30% RH (see Figure 4C). The stabilization time was achieved after 30 min (see Figure 4C), with a H_2O uptake of ∼4.5 wt % (at 30% RH, the water uptake was 4.2 wt %, see Figure 2). Then, at approximately 50 min, the CO_2 flow was initiated and the weight increase was very small, reaching a total CO_2 capture of only 0.4 wt %. This result means that at 30% RH, the sample is practically saturated with H_2O and that it is not possible to capture CO_2 (see Figure 4C).

As we mentioned before, NOTT-401 shows a pore diameter of 6.3 Å,[14] which corresponds to the microporous regime. In contrast, Llewellyn and co-workers[13] reported an outstanding result of a 5-fold increase in CO_2 uptake on a mesoporous

DOI: 10.1021/acsomega.6b00102
ACS Omega 2016, 1, 305−310

material (MIL-100(Fe)). The MIL-100(Fe) structure consists of two types of cages with access windows of approximately 25 and 29 Å,[13] which are considerably larger than the micropores exhibited by NOTT-401. Therefore, at 30% RH, the saturation with H_2O molecules of these micropores, in NOTT-401, was almost complete, and consequently, the incorporation of CO_2 molecules into the micropores was not viable. This rationalization is based on experimental evidence obtained from another microporous material previously reported by us.[19d] Additionally, this experimental evidence is supported by Medders and Paesani[22] who carried out an in silico infrared spectroscopy study of the behavior of H_2O molecules confined in a microporous coordination polymer entitled MIL-53(Cr). The MIL-53(Cr) structure is based on a series of one-dimensional chains conformed of $CrO_4(\mu_2\text{-OH})$ octahedra sharing its corners, linked by 1,4-benzenedicarboxylate (BDC) ligands.[23] Then, Paesani showed[22] two different scenarios where, depending on the amount of H_2O adsorbed in the material, the location of water molecules inside of the channels of MIL-53(Cr) is rather different.

In the first case, when there is low water loading in the pore, the H_2O molecules interact strongly with the pore walls, through the formation of hydrogen bonds with the μ_2-OH functional groups, and this produces a very ordered and homogeneous organization of the H_2O molecules inside of the pore channels. This was also corroborated by Haigis[16] who demonstrated by molecular dynamics (MD) that at low water loadings, the water molecules and the hydroxo functional groups (μ_2-OH) within the pore form very stable hydrogen bonds in MIL-53(Cr). Furthermore, using GCMC simulations on MIL-53(Cr), Maurin et al.[24] showed that at low water loadings, these molecules are uniformly distributed at the inner surface of the material.

In the second case, at higher water loadings, intermolecular interactions between the H_2O molecules become considerably stronger, and, conversely to the first case, the arrangement of water molecules is neither homogeneous nor ordered inside of the material. In other words, at low H_2O loadings, the channels of MIL-53(Cr) present a very regular and well-ordered template for packing water molecules more regularly and efficiently, and therefore these H_2O molecules enhance the total CO_2 uptake by providing a hydrogen bond to the CO_2 molecules.

CONCLUSIONS

Summarizing, the water-stable NOTT-401 showed interesting water adsorption properties that provided us a guideline to evaluate the amount of water needed for a better CO_2 sequestration. Thus, finding the most suitable partial saturation of H_2O molecules (percentage of RH) into the micropores of NOTT-401 is fundamental to improving the CO_2 uptake. As previously described by Paesani,[22] Haigis,[16] and Maurin,[24] via computational calculations, at low water loadings (in microporous materials that show bridging hydroxo functional groups), these H_2O molecules can be accommodated very efficiently by taking advantage of the relatively strong hydrogen bond with the μ_2-OH functional group. Consequently, these H_2O molecules enhance the total CO_2 uptake by providing a hydrogen bond to the CO_2 molecules, as we have experimentally demonstrated. Thus, our experimental evidence corroborates that the CO_2 confinement effects induced by H_2O[20] can take place inside of the NOTT-401 micropores, enhancing the total CO_2 uptake. After testing different RH conditions (5, 20, and 30% RH), we found that the maximum CO_2 capture was achieved at the lowest RH (5% RH), with a total amount of CO_2 capture of roughly 3.9 wt %. Remarkably, the CO_2 capture under humid conditions presents a 3.2-fold increase when compared with that under anhydrous conditions (1.2 wt %).

ASSOCIATED CONTENT

Supporting Information

The Supporting Information is available free of charge on the ACS Publications website at DOI: 10.1021/acsomega.6b00102.

TGA data, PXRDP data, Henry's law calculations, and uptake experiments (PDF)

AUTHOR INFORMATION

Corresponding Authors

*E-mail: egz@xanum.uam.mx (E.G.-Z.).
*E-mail: argel@unam.mx (I.A.I.).

Notes

The authors declare no competing financial interest.

ACKNOWLEDGMENTS

The authors thank CONACyT Mexico (212318) and PAPIIT UNAM Mexico (IN100415) for financial support. E.S.-G. thanks CONACyT Mexico (grant 289042). J.B. thanks SEP-CONACyT (154626) and UNAM-DGAPA-PAPIIT (IG-100315). E.G.-Z. thanks CONACyT (236879), Mexico, for financial support. The authors thank U. Winnberg (ITAM) for scientific discussions.

REFERENCES

(1) Olivier, J. G. J.; Janssens-Maenhout, G.; Muntean, M.; Peters, J. A. H. W. *Trends in Global CO_2 Emissions*: 2015 Report; PBL Netherlands Environmental Assessment Agency: The Hague, 2015; pp 4−5.

(2) (a) Keskin, S.; van Heest, T. M.; Sholl, D. S. Can metal-organic framework materials play a useful role in large-scale carbon dioxide separations? *ChemSusChem* **2010**, *3*, 879−891. (b) Sumida, K.; Rogow, D. L.; Mason, J. A.; McDonald, T. M.; Bloch, E. D.; Herm, Z. R.; Bae, T.-H.; Long, J. R. Carbon Dioxide Capture in Metal-Organic Frameworks. *Chem. Rev.* **2012**, *112*, 724−781. (c) Liu, J.; Thallapally, P. K.; McGrail, B. P.; Brown, D. R.; Liu, J. Progress in adsorption-based CO_2 capture by metal−organic frameworks. *Chem. Soc. Rev.* **2012**, *41*, 2308−2322.

(3) (a) Küsgens, P.; Rose, M.; Senkovska, I.; Fröde, H.; Henschel, A.; Siegle, S.; Kaskel, S. Characterization of metal-organic frameworks by water adsorption. *Microporous Mesoporous Mater.* **2009**, *120*, 325−330. (b) Low, J. J.; Benin, A. I.; Jakubczak, P.; Abrahamian, J. F.; Faheem, S. A.; Willis, R. R. Virtual High Throughput Screening Confirmed Experimentally: Porous Coordination Polymer Hydration. *J. Am. Chem. Soc.* **2009**, *131*, 15834−15842.

(4) (a) Burtch, N. C.; Jasuja, H.; Walton, K. S. Water Stability and Adsorption in Metal−Organic Frameworks. *Chem. Rev.* **2014**, *114*, 10575−10612. (b) Canivet, J.; Fateeva, A.; Guo, Y.; Coasne, B.; Farrusseng, D. Water adsorption in MOFs: Fundamentals and applications. *Chem. Soc. Rev.* **2014**, *43*, 5594−5617.

(5) Cavka, J. H.; Jakobsen, S.; Olsbye, U.; Guillou, N.; Lamberti, C.; Bordiga, S.; Lillerud, K. P. A New Zirconium Inorganic Building Brick Forming Metal Organic Frameworks with Exceptional Stability. *J. Am. Chem. Soc.* **2008**, *130*, 13850−13851.

(6) Furukawa, H.; Gándara, F.; Zhang, Y.-B.; Jiang, J.; Queen, W. L.; Hudson, M. R.; Yaghi, O. M. Water Adsorption in Porous Metal−Organic Frameworks and Related Materials. *J. Am. Chem. Soc.* **2014**, *136*, 4369−4381.

DOI: 10.1021/acsomega.6b00102
ACS Omega 2016, 1, 305−310

(7) (a) Wang, T. C.; Bury, W.; Gómez-Gualdrón, D. A.; Vermeulen, N. A.; Mondloch, J. E.; Deria, P.; Zhang, K.; Moghadam, P. Z.; Sarjeant, A. A.; Snurr, R. Q.; Stoddart, J. F.; Hupp, J. T.; Farha, O. K. Ultrahigh Surface Area Zirconium MOFs and Insights into the Applicability of the BET Theory. *J. Am. Chem. Soc.* **2015**, *137*, 3585−3591. (b) Deria, P.; Gómez-Gualdrón, D. A.; Bury, W.; Schaef, H. T.; Wang, T. C.; Thallapally, P. K.; Sarjeant, A. A.; Snurr, R. Q.; Hupp, J. T.; Farha, O. K. Ultraporous, Water Stable, and Breathing Zirconium-Based Metal−Organic Frameworks with ftw Topology. *J. Am. Chem. Soc.* **2015**, *137*, 13183−13190.

(8) (a) Jasuja, H.; Huang, Y.-g.; Walton, K. S. Adjusting the Stability of Metal−Organic Frameworks under Humid Conditions by Ligand Functionalization. *Langmuir* **2012**, *28*, 16874−16880. (b) Jasuja, H.; Zang, J.; Sholl, D. S.; Walton, K. S. Rational tuning of water vapor and CO_2 adsorption in highly stable Zr-based MOFs. *J. Phys. Chem. C* **2012**, *116*, 23526−23532. (c) Jasuja, H.; Jiao, Y.; Burtch, N. C.; Huang, Y.-g.; Walton, K. S. Synthesis of Cobalt-, Nickel-, Copper-, and Zinc-Based, Water-Stable, Pillared Metal−Organic Frameworks. *Langmuir* **2014**, *30*, 14300−14307.

(9) Zheng, B.; Lin, X.; Wang, Z.; Yun, R.; Fan, Y.; Ding, M.; Hu, X.; Yi, P. Enhanced water stability of a microporous acylamide-functionalized metal−organic framework via interpenetration and methyl decoration. *CrystEngComm* **2014**, *16*, 9586−9589.

(10) Wittmann, T.; Siegel, R.; Reimer, N.; Milius, W.; Stock, N.; Senker, J. Enhancing the Water Stability of Al-MIL-101-NH_2 via Postsynthetic Modification. *Chem.—Eur. J.* **2015**, *21*, 314−323.

(11) Andirova, D.; Lei, Y.; Zhao, X.; Choi, S. Functionalization of Metal-Organic Frameworks for Enhanced Stability under Humid Carbon Dioxide Capture Conditions. *ChemSusChem* **2015**, *8*, 3405−3409.

(12) (a) Llewellyn, P. L.; Bourrelly, S.; Serre, C.; Filinchuk, Y.; Férey, G. How hydration drastically improves adsorption selectivity for CO_2 over CH_4 in the flexible chromium terephthalate MIL-53. *Angew. Chem., Int. Ed.* **2006**, *45*, 7751−7754. (b) Yazaydın, A. Ö.; Benin, A. I.; Faheem, S. A.; Jakubczak, P.; Low, J. J.; Willis, R. R.; Snurr, R. Q. Enhanced CO_2 Adsorption in Metal-Organic Frameworks via Occupation of Open-Metal Sites by Coordinated Water Molecules. *Chem. Mater.* **2009**, *21*, 1425−1430.

(13) Soubeyrand-Lenoir, E.; Vagner, C.; Yoon, J. W.; Bazin, P.; Ragon, F.; Hwang, Y. K.; Serre, C.; Chang, J.-S.; Llewellyn, P. L. How water fosters a remarkable 5-fold increase in low-pressure CO_2 uptake within mesoporous MIL-100(Fe). *J. Am. Chem. Soc.* **2012**, *134*, 10174−10181.

(14) Ibarra, I. A.; Yang, S.; Lin, X.; Blake, A. J.; Rizkallah, P. J.; Nowell, H.; Allan, D. R.; Champness, N. R.; Hubberstey, P.; Schröder, M. Highly porous and robust scandium-based metal−organic frameworks for hydrogen storage. *Chem. Commun.* **2011**, *47*, 8304−8306.

(15) (a) Zhao, X.; Xiao, B.; Fletcher, A. J.; Thomas, K. M.; Bradshaw, D.; Rosseinsky, M. J. Hysteretic Adsorption and Desorption of Hydrogen by Nanoporous Metal-Organic Frameworks. *Science* **2004**, *306*, 1012−1015. (b) Choi, H. J.; Dincă, M.; Long, J. R. Broadly Hysteretic H_2 Adsorption in the Microporous Metal−Organic Framework Co(1,4-benzenedipyrazolate). *J. Am. Chem. Soc.* **2008**, *130*, 7848−7850.

(16) Haigis, V.; Coudert, F.-X.; Vuilleumier, R.; Boutin, A. Investigation of structure and dynamics of the hydrated metal−organic framework MIL-53(Cr) using first-principles molecular dynamics. *Phys. Chem. Chem. Phys.* **2013**, *15*, 19049−19056.

(17) (a) Ruthven, D. M. Adsorption and Diffusion. In *Molecular Sieves*; Science and Technology Series; Karge, H. G., Weitkamp, J., Eds.; Springer-Verlag: Berlin, 2008; Vol. 7, p 5. (b) *CRC Handbook of Chemistry and Physics*, 96th ed.; Haynes, W. M., Ed.; CRC Press, Taylor & Francis Group: Boca Raton, 2015; p 6−53.

(18) O'koye, I. P.; Benham, M.; Thomas, K. M. Adsorption of Gases and Vapors on Carbon Molecular Sieves. *Langmuir* **1997**, *13*, 4054−4059.

(19) (a) Gonzalez, M. R.; González-Estefan, J. H.; Lara-García, H. A.; Sánchez-Camacho, P.; Basaldella, E. I.; Pfeiffer, H.; Ibarra, I. A. Separation of CO_2 from CH_4 and CO_2 capture in the presence of water vapour in NOTT-400. *New J. Chem.* **2015**, *39*, 2400−2403. (b) Lara-García, H. A.; Gonzalez, M. R.; González-Estefan, J. H.; Sánchez-Camacho, P.; Lima, E.; Ibarra, I. A. Removal of CO_2 from CH_4 and CO_2 capture in the presence of H_2O vapour in NOTT-401. *Inorg. Chem. Front.* **2015**, *2*, 442−447. (c) Peralta, R. A.; Alcántar-Vázquez, B.; Sánchez-Serratos, M.; González-Zamora, E.; Ibarra, I. A. Carbon dioxide capture in the presence of water vapour in InOF-1. *Inorg. Chem. Front.* **2015**, *2*, 898−903. (d) Álvarez, J. R.; Peralta, R. A.; Balmaseda, J.; González-Zamora, E.; Ibarra, I. A. Water adsorption properties of a Sc(III) porous coordination polymer for CO_2 capture applications. *Inorg. Chem. Front.* **2015**, *2*, 1080−1084. (e) Sánchez-Serratos, M.; Bayliss, P. A.; Peralta, R. A.; González-Zamora, E.; Lima, E.; Ibarra, I. A. CO_2 capture in the presence of water vapour in MIL-53(Al). *New J. Chem.* **2016**, *40*, 68−72. (f) Zárate, A.; Peralta, R. A.; Bayliss, P. A.; Howie, R.; Sánchez-Serratos, M.; Carmona-Monroy, P.; Solis-Ibarra, D.; González-Zamora, E.; Ibarra, I. A. CO_2 capture under humid conditions in NH_2-MIL-53(Al): The influence of the amine functional group. *RSC Adv.* **2016**, *6*, 9978−9983. (g) Peralta, R. A.; Campos-Reales-Pineda, A.; Pfeiffer, H.; Álvarez, J. R.; Zárate, J. A.; Balmaseda, J.; González-Zamora, E.; Martínez, A.; Martínez-Otero, D.; Jancik, V.; Ibarra, I. A. CO_2 capture enhancement in InOF-1 via the bottleneck effect of confined ethanol. *Chem. Commun.* **2016**, *52*, 10273−10276.

(20) (a) Ho, N. L.; Porcheron, F.; Pellenq, R. J.-M. Experimental and Molecular Simulation Investigation of Enhanced CO_2 Solubility in Hybrid Adsorbents. *Langmuir* **2010**, *26*, 13287−13296. (b) Ho, L. N.; Pellitero, J. P.; Porcheron, F.; Pellenq, R. J.-M. Enhanced CO_2 Solubility in Hybrid MCM-41: Molecular Simulations and Experiments. *Langmuir* **2011**, *27*, 8187−8197. (c) Ho, L. N.; Clauzier, S.; Schuurman, Y.; Farrusseng, D.; Coasne, B. Gas uptake in solvents confined in mesopores: Adsorption versus enhanced solubility. *J. Phys. Chem. Lett.* **2013**, *4*, 2274−2278.

(21) (a) Liedl, K. R.; Sekušak, S.; Mayer, E. Has the Dimer of Carbonic Acid a Lower Energy Than Its Constituents Water and Carbon Dioxide? *J. Am. Chem. Soc.* **1997**, *119*, 3782−3784. (b) Tho, N. M.; Ha, T. K. A theoretical study of the formation of carbonic acid from the hydration of carbon dioxide: A case of active solvent catalysis. *J. Am. Chem. Soc.* **1984**, *106*, 599−602. (c) Yang, S. O.; Yang, I. M.; Kim, Y. S.; Lee, C. S. Measurement and prediction of phase equilibria for water + CO_2 in hydrate forming conditions. *Fluid Phase Equilib.* **2000**, *175*, 75−89. (d) Duan, Z.; Sun, R. An improved model calculating CO_2 solubility in pure water and aqueous NaCl solutions from 273 to 533 K and from 0 to 2000 bar. *Chem. Geol.* **2003**, *193*, 257−271. (e) Rege, S. U.; Yang, R. T. A novel FTIR method for studying mixed gas adsorption at low concentrations: H_2O and CO_2 on NaX zeolite and γ-alumina. *Chem. Eng. Sci.* **2001**, *56*, 3781−3796. (f) Baltrusaitis, J.; Schuttlefield, J. D.; Zeitler, E.; Jensen, J. H.; Grassian, V. H. Surface Reactions of Carbon Dioxide at the Adsorbed Water−Oxide Interface. *J. Phys. Chem. C* **2007**, *111*, 14870−14880. (g) Bai, R.; Yang, R. T. A Modification of the Doong−Yang Model for Gas Mixture Adsorption Using the Lewis Relationship. *Langmuir* **2005**, *21*, 8326−8332. (h) Li, G.; Xiao, P.; Webley, P. Binary Adsorption Equilibrium of Carbon Dioxide and Water Vapor on Activated Alumina. *Langmuir* **2009**, *25*, 10666−10675.

(22) Medders, G. R.; Paesani, F. Water dynamics in metal−organic frameworks: Effects of heterogeneous confinement predicted by computational spectroscopy. *J. Phys. Chem. Lett.* **2014**, *5*, 2897−2902.

(23) Serre, C.; Millange, F.; Thouvenot, C.; Nogués, M.; Marsolier, G.; Louër, D.; Férey, G. Very Large Breathing Effect in the First Nanoporous Chromium(III)-Based Solids: MIL-53 or $Cr^{III}(OH)\cdot\{O_2C-C_6H_4-CO_2\}\cdot\{HO_2C-C_6H_4-CO_2H\}_x\cdot H_2O_y$. *J. Am. Chem. Soc.* **2002**, *124*, 13519−13526.

(24) Salles, F.; Bourrelly, S.; Jobic, H.; Devic, T.; Guillerm, V.; Llewellyn, P.; Serre, C.; Ferey, G.; Maurin, G. Molecular Insight into the Adsorption and Diffusion of Water in the Versatile Hydrophilic/Hydrophobic Flexible MIL-53(Cr) MOF. *J. Phys. Chem. C* **2011**, *115*, 10764−10776.

DOI: 10.1021/acsomega.6b00102
ACS Omega 2016, 1, 305−310